Few-Body Systems 28, 15–34 (2000)

Few-Body Systems

Three-Body Scattering Below Breakup Threshold: An Approach Without Using Partial Waves

W. Schadow[1,*], Ch. Elster[1], and W. Glöckle[2]

[1] Institute of Nuclear and Particle Physics, and Department of Physics, Ohio University, Athens, OH 45701, USA
[2] Institut für Theoretische Physik II, Ruhr-Universität Bochum, D-44780 Bochum, Germany

Abstract. The Faddeev equation for three-body scattering below the three-body breakup threshold is directly solved without employing a partial-wave decomposition. In the simplest form it is a three-dimensional integral equation in four variables. From its solution the scattering amplitude is obtained as function of vector Jacobi momenta. Based on Malfliet-Tjon-type potentials differential and total cross sections are calculated. The numerical stability of the algorithm is demonstrated and the properties of the scattering amplitude discussed.

1 Introduction

Traditionally three-nucleon scattering calculations are carried out by solving Faddeev equations in a partial-wave truncated basis. A partial-wave decomposition replaces the continuous angle variables by discrete orbital angular-momentum quantum numbers, and thus reduces the number of continuous variables, which have to be discretized in a numerical treatment. For low projectile energies the procedure of considering orbital angular-momentum components appears physically justified due to arguments related to the centrifugal barrier. However, the algebraic and algorithmic steps to be carried out in a partial-wave decomposition can be quite involved when solving the Faddeev equations. If one considers three-nucleon scattering at a few hundred MeV projectile energy, the number of partial waves needed to achieve convergence proliferates, and limitations with respect to computational feasibility and accuracy are reached. The amplitudes acquire stronger angular dependence, which is already visible in the two-nucleon amplitudes, and their formation by an increasing number of partial waves not only becomes more tedious but also less informative. The method of partial-wave decomposition looses its physical transparency, and the direct use of angular variables becomes more appealing.

* *Present address*: TRIUMF, 4004 Wesbrook Mall, Vancouver, B.C. V6T 2A3, Canada

It appears therefore natural to avoid a partial-wave representation completely and work directly with vector variables. This is common practice in bound-state calculations of few-nucleon systems based on variational [1] and Green's function Monte Carlo (GFMC) methods [2–5], which are carried out in configuration space.

Our aim is to work directly with vector variables in the Faddeev scheme in momentum space. In ref. [6] we demonstrated for Malfliet-Tjon-type potentials that the two-body Lippmann-Schwinger equation can readily be solved in momentum space as function of vector momenta. At intermediate energies the strong forward peaking of the t-matrix was quite easily achieved through the angular variable but required relatively many partial-wave contributions. The choice of momentum vectors as adequate variables is also suggested by the nucleon-nucleon (NN) force. Here the dependence on momentum vectors can be rather simple, e.g. in the widely used one-boson-exchange force, whereas the partial-wave representation of this force leads to rather complicated expressions [7].

In ref. [8] we showed that the bound-state Faddeev equation has a rather transparent structure when formulated with vector variables compared to the coupled set of two-dimensional integral equations obtained in a partial-wave decomposed form. Based on Malfliet-Tjon-type interactions it was demonstrated that the numerical solution of the bound-state equation using vector variables is straightforward and numerically very accurate.

In this article we want to show that the solution of the three-body scattering equation can also be obtained in a straightforward manner when employing vector variables, i.e. magnitudes of momenta and angles between the momentum vectors. In this work we concentrate on scattering below the three-body breakup threshold. Though we avoid the singularity of the free three-body propagator, we already encounter the two-body fragmentation cut related to the pole in the two-body t-matrix. As a further simplification we neglect spin and iso-spin degrees of freedom and treat three-boson scattering. The interactions employed are of Yukawa type, and no separable approximations are involved. The Faddeev equation for three identical bosons is solved exactly as function of momentum vectors. To the best of our knowledge this is the first time such an approach is carried out.

This article is organized as follows. Sect. 2 describes our choice of momentum and angle variables for the unknown amplitude in the Faddeev equation and the integral kernel of that equation. The calculation of the only scattering observable, the differential cross section is also derived. In Sect. 3 we discuss details of our algorithms and numerical procedures and present our results. In addition properties of the Faddeev amplitude are displayed. In Sect. 4 we discuss an alternative choice of variables and demonstrate that this choice leads to the same result as the choice of Sect. 2. We conclude in Sect. 5.

2 Three-Body Scattering Equations

We solve the Faddeev equations for three identical particles in the form

$$T|\phi\rangle = tP|\phi\rangle + tG_0PT|\phi\rangle, \tag{1}$$

where t is the two-body t-matrix defined in the subsystem and the operator P is the sum of a cyclic and an anticyclic permutation of three objects. The initial channel state $|\phi\rangle$ is composed of a deuteron $|\varphi_d\rangle$ and the momentum eigenstate $|\mathbf{q}_0\rangle$ of the projectile nucleon. The free three-nucleon propagator is given by $G_0 = (E - H_0 + i\varepsilon)^{-1}$, with E being the total centre-of-mass (c.m.) energy

$$E = \frac{3}{4m} q_0^2 + E_d. \tag{2}$$

Here E_d is the binding energy of the two-body subsystem. Since we work below the three-particle breakup threshold we only need to consider the operator for elastic scattering

$$U = PG_0^{-1} + PT. \tag{3}$$

From U one obtains the differential cross section for elastic scattering [9] as

$$\frac{d\sigma}{d\Omega} = \left(\frac{2}{3}m\right)^2 (2\pi)^4 |\langle \mathbf{q}' \varphi_d | U | \mathbf{q}_0 \varphi_d \rangle|^2, \tag{4}$$

where $|\mathbf{q}'| = |\mathbf{q}_0|$. The total cross section is either obtained by integrating over the angle variable

$$\sigma_{\text{tot}}^{\text{el}} = \int d\Omega \frac{d\sigma^{\text{el}}}{d\Omega} = \left(\frac{2}{3}m\right)^2 (2\pi)^5 \int_{-1}^{1} dx' |\langle q_0 x' \varphi_d | U | \mathbf{q}_0 \varphi_d \rangle|^2 \tag{5}$$

or via the optical theorem

$$\sigma_{\text{tot}} = -(2\pi)^3 \frac{4m}{3q_0} \text{Im}(\langle \mathbf{q}_0 \varphi_d | U | \mathbf{q}_0 \varphi_d \rangle). \tag{6}$$

In order to solve Eq. (1) we introduce the standard Jacobi momenta $\mathbf{p}$, the relative momentum in the subsystem, and $\mathbf{q}$, the relative momentum of the spectator with respect to the subsystem. With $|\phi\rangle = |\mathbf{q}_0 \varphi_d\rangle$ Eq. (1) reads

$$\langle \mathbf{pq} | T | \mathbf{q}_0 \varphi_d \rangle = \langle \mathbf{pq} | tP | \mathbf{q}_0 \varphi_d \rangle + \langle \mathbf{pq} | tG_0 PT | \mathbf{q}_0 \varphi_d \rangle. \tag{7}$$

The driving term of Eq. (1) is given by

$$\begin{aligned} \langle \mathbf{pq} | tP | \phi \rangle &= \int d^3q' d^3p' d^3q'' d^3p'' \langle \mathbf{pq} | t | \mathbf{p}'\mathbf{q}' \rangle \langle \mathbf{p}'\mathbf{q}' | P | \mathbf{p}''\mathbf{q}'' \rangle \langle \mathbf{p}''\mathbf{q}'' | \phi \rangle \\ &= \int d^3q' d^3p' d^3p'' \langle \mathbf{pq} | t | \mathbf{p}'\mathbf{q}' \rangle \langle \mathbf{p}'\mathbf{q}' | P | \mathbf{p}''\mathbf{q}_0 \rangle \langle \mathbf{p}'' | \varphi_d \rangle. \end{aligned} \tag{8}$$

The momentum states are normalized according to $\langle \mathbf{p}'\mathbf{q}' | \mathbf{pq} \rangle = \delta^3(\mathbf{p}' - \mathbf{p}) \delta^3(\mathbf{q}' - \mathbf{q})$. To evaluate the permutation operator $P = P_{12}P_{23} + P_{13}P_{23}$ explicitly, the Jacobi coordinates in the different subsystems (12) and (13) need to

be expressed through those defined in the subsystems (23), which gives

$$\begin{aligned}
\mathbf{q}_1 &= -\mathbf{p}_2 - \tfrac{1}{2}\mathbf{q}_2, \\
\mathbf{p}_1 &= -\tfrac{1}{2}\mathbf{p}_2 + \tfrac{3}{4}\mathbf{q}_2, \\
\mathbf{q}_1 &= \mathbf{p}_3 - \tfrac{1}{2}\mathbf{q}_3, \\
\mathbf{p}_1 &= -\tfrac{1}{2}\mathbf{p}_3 - \tfrac{3}{4}\mathbf{q}_3.
\end{aligned} \tag{9}$$

Then the permutation operator occurring in Eq. (8) can be evaluated as

$$\begin{aligned}
\langle \mathbf{p}'\mathbf{q}'|P|\mathbf{p}''\mathbf{q}''\rangle &= \langle \mathbf{p}'\mathbf{q}'|\mathbf{p}''\mathbf{q}''\rangle_2 + \langle \mathbf{p}'\mathbf{q}'|\mathbf{p}''\mathbf{q}''\rangle_3 \\
&= \delta^3(\mathbf{p}' + \tfrac{1}{2}\mathbf{q}' + \mathbf{q}'')\delta^3(\mathbf{p}'' - \mathbf{q}' - \tfrac{1}{2}\mathbf{q}'') \\
&\quad + \delta^3(\mathbf{p}' - \tfrac{1}{2}\mathbf{q}' - \mathbf{q}'')\delta^3(\mathbf{p}'' + \mathbf{q}' + \tfrac{1}{2}\mathbf{q}'').
\end{aligned} \tag{10}$$

The indices 2 and 3 indicate the corresponding subsystem (for more details see ref. [8]). Inserting this relation into Eq. (8) reduces the driving term to

$$\langle \mathbf{pq}|tP|\phi\rangle = t_s\left(\mathbf{p}, \frac{1}{2}\mathbf{q} + \mathbf{q}_0; E - \frac{3}{4m}q^2\right)\varphi_d(|\mathbf{q} + \tfrac{1}{2}\mathbf{q}_0|), \tag{11}$$

where $t_s(\mathbf{p}, \mathbf{q}, E)$ is the symmetrized two-nucleon t-matrix,

$$t_s(\mathbf{p}, \mathbf{q}, E) = t(\mathbf{p}, \mathbf{q}, E) + t(-\mathbf{p}, \mathbf{q}, E). \tag{12}$$

Since we neglect spin, the deuteron consists only of an S-state, and thus the wave function depends only on the magnitude of the momenta.

Carrying out a similar calculation for the integral term in Eq. (7) leads to the explicit form of the Faddeev equation

$$\begin{aligned}
\langle \mathbf{pq}|T|\mathbf{q}_0\varphi_d\rangle &= t_s\left(\mathbf{p}, \frac{1}{2}\mathbf{q} + \mathbf{q}_0; E - \frac{3}{4m}q^2\right)\varphi_d(|\mathbf{q} + \tfrac{1}{2}\mathbf{q}_0|) \\
&\quad + \int d^3q'' \frac{t_s\left(\mathbf{p}, \frac{1}{2}\mathbf{q} + \mathbf{q}''; E - \frac{3}{4m}q^2\right)}{E - \frac{1}{m}(q^2 + \mathbf{q}\cdot\mathbf{q}'' + q''^2)} \langle \mathbf{q} + \tfrac{1}{2}\mathbf{q}'', \mathbf{q}''|T|\mathbf{q}_0\varphi_d\rangle.
\end{aligned} \tag{13}$$

The transition operator T is needed for all values of $\mathbf{q}$. Thus one encounters the pole of the two-body t-matrix at the bound-state energy E_d. Extracting explicitly the residue by defining

$$t_s(\mathbf{p}, \mathbf{q}, E) = \frac{\hat{t}_s(\mathbf{p}, \mathbf{q}, E)}{E - E_d} \tag{14}$$

and similarly for T, Eq. (13) can be written as

$$\begin{aligned}
\langle \mathbf{pq}|\hat{T}|\mathbf{q}_0\varphi_d\rangle &= \hat{t}_s\left(\mathbf{p}, \frac{1}{2}\mathbf{q} + \mathbf{q}_0; E - \frac{3}{4m}q^2\right)\varphi_d(|\mathbf{q} + \tfrac{1}{2}\mathbf{q}_0|) \\
&\quad + \int d^3q'' \frac{\hat{t}_s\left(\mathbf{p}, \frac{1}{2}\mathbf{q} + \mathbf{q}''; E - \frac{3}{4m}q^2\right)}{E - \frac{1}{m}(q^2 + \mathbf{q}\cdot\mathbf{q}'' + q''^2)} \frac{\langle \mathbf{q} + \frac{1}{2}\mathbf{q}'', \mathbf{q}''|\hat{T}|\mathbf{q}_0\varphi_d\rangle}{E - \frac{3}{4m}q''^2 - E_d + i\varepsilon}.
\end{aligned} \tag{15}$$

This expression is the starting point for our numerical calculation of the transition amplitude. Correspondingly the operator for elastic scattering in Eq. (3) reads

$$\langle \mathbf{q}'\varphi_d|U|\mathbf{q}_0\varphi_d\rangle = 2\varphi_d\left(\tfrac{1}{2}\mathbf{q}'+\mathbf{q}_0\right)\left(E-\frac{1}{m}(q'^2+\mathbf{q}'\cdot\mathbf{q}_0+q_0^2)\right)\varphi_d(\mathbf{q}'+\tfrac{1}{2}\mathbf{q}_0) + 2\int d^3q''\varphi_d\left(\tfrac{1}{2}\mathbf{q}'+\mathbf{q}''\right)\left\langle \mathbf{q}'+\tfrac{1}{2}\mathbf{q}'', \mathbf{q}''|T|\mathbf{q}_0\varphi_d\right\rangle. \tag{16}$$

The transition amplitude $\hat{T}$ as given in Eq. (15) depends on the vector variables $\mathbf{q}_0$, $\mathbf{q}$, and $\mathbf{p}$. Going to c.m. coordinates and choosing the z-axis in the direction of $\mathbf{q}_0$ we are left with five independent variables. Those are the magnitudes of the vectors $\mathbf{q}$ and $\mathbf{p}$, their angles with respect to the z-axis and the azimuthal angle φ_{pq} between them. The vectors $\mathbf{q}_0$ and $\mathbf{q}$ define the x-z plane in a Cartesian coordinate system. In these variables the matrix element for the transition amplitude can be written as $\langle p, x_p, \cos\varphi_{pq}, q, x_q|T|\mathbf{q}_0\varphi_d\rangle$ with

$$\begin{aligned} p &= |\mathbf{p}|,\\ q &= |\mathbf{q}|,\\ x_p &= \hat{\mathbf{p}}\cdot\hat{\mathbf{q}}_0,\\ x_q &= \hat{\mathbf{q}}\cdot\hat{\mathbf{q}}_0,\\ \cos\varphi_{pq} &= \cos\varphi(\mathbf{p},\mathbf{q}) = \hat{\mathbf{p}}_{xy}\cdot\hat{\mathbf{q}}_{xy}. \end{aligned} \tag{17}$$

The index xy denotes the projection of the vectors into the x-y plane. In order to obtain the matrix elements $\langle \mathbf{pq}|\hat{T}|\mathbf{q}_0\varphi_d\rangle$, Eq. (15) needs to be solved. For the integration we choose the z-axis parallel to $\mathbf{q}$. This implies that the azimuthal angle φ between $(\mathbf{q}+\frac{1}{2}\mathbf{q}'')$ and $\mathbf{q}''$ for $\langle \mathbf{q}+\frac{1}{2}\mathbf{q}'', \mathbf{q}''|\hat{T}|\mathbf{q}_0\varphi_d\rangle$ in the kernel of Eq. (15) is zero, and thus $\cos\varphi_{pq}=1$ in Eq. (17). This also means that we only need to solve Eq. (15) for $\cos\varphi_{pq}=1$, or in other words, that $\mathbf{p}$ lies in the same plane that is spanned by $\mathbf{q}$ and $\mathbf{q}''$. From these considerations follows that we only have to solve Eq. (15) for $\langle p, x_p, 1, q, x_q|\hat{T}|\mathbf{q}_0\varphi_d\rangle$, i.e. for *four* independent variables instead of five, as it could be assumed from the considerations proceeding Eq. (17). Thus, for our calculations we arrive from Eq. (17) with $\cos\varphi_{pq}=1$ at the following two additional angle variables

$$\begin{aligned} x_{pq} &= \hat{\mathbf{p}}\cdot\hat{\mathbf{q}} = x_px_q+\sqrt{1-x_p^2}\sqrt{1-x_q^2}\cos\varphi_{pq} = x_px_q+\sqrt{1-x_p^2}\sqrt{1-x_q^2},\\ x'' &= \hat{\mathbf{q}}\cdot\hat{\mathbf{q}}''. \end{aligned} \tag{18}$$

The angle variables x_p and x_q are already given in Eq. (17). The momenta occurring in Eq. (15) are now given explicitly as

$$\begin{aligned} |\tfrac{1}{2}\mathbf{q}+\mathbf{q}_0| &= \sqrt{\tfrac{1}{4}q^2+qq_0x_q+q_0^2}, \qquad |\tfrac{1}{2}\mathbf{q}+\mathbf{q}''| = \sqrt{\tfrac{1}{4}q^2+qq''x''+q''^2},\\ |\mathbf{q}+\tfrac{1}{2}\mathbf{q}_0| &= \sqrt{q^2+qq_0x_q+\tfrac{1}{4}q_0^2}, \qquad |\mathbf{q}+\tfrac{1}{2}\mathbf{q}''| = \sqrt{q^2+qq''x''+\tfrac{1}{4}q''^2}. \end{aligned} \tag{19}$$

Expressions for the remaining angle variables can be found in Appendix A. Inserting all variables into Eq. (15), the final expression for the transition amplitude reads

$$
\begin{aligned}
&\langle p, x_p, 1, q, x_q | \hat{T} | \mathbf{q}_0 \varphi_d \rangle \\
&\quad = \varphi_d\left(\sqrt{q^2 + q q_0 x_q + \tfrac{1}{4} q_0^2}\right) \\
&\qquad \times \hat{t}_s\left(p, \sqrt{\tfrac{1}{4} q^2 + q q_0 x_q + q_0^2}, \frac{\frac{1}{2} q x_{pq} + q_0 x_p}{\sqrt{\frac{1}{4} q^2 + q q_0 x_q + q_0^2}}; E - \frac{3}{4m} q^2\right) \\
&\qquad + \int_0^\infty dq'' q''^2 \int_{-1}^{1} dx'' \int_0^{2\pi} d\varphi'' \, \frac{1}{E - \dfrac{1}{m}(q^2 + q q'' x'' + q''^2)} \\
&\qquad \times \hat{t}_s\left(p, \sqrt{\tfrac{1}{4} q^2 + q q'' x'' + q''^2}, \frac{\frac{1}{2} q x_{pq} + q'' y_p}{\sqrt{\frac{1}{4} q^2 + q q'' x'' + q''^2}}; E - \frac{3}{4m} q^2\right) \\
&\qquad \times \frac{\left\langle \sqrt{q^2 + q q'' x'' + \frac{1}{4} q''^2}, \frac{q x_q + \frac{1}{2} q'' y_{q_0}}{\sqrt{q^2 + q q'' x'' + \frac{1}{4} q''^2}}, 1, q'', y_{q_0} | \hat{T} | \mathbf{q}_0 \varphi_d \right\rangle}{E - \dfrac{3}{4m} q''^2 - E_d + i\varepsilon}.
\end{aligned}
\tag{20}
$$

This is a three-dimensional integral equation in four variables, namely p, x_p, q, and x_q. The advantage of our choice of the coordinate system is that the free propagator has a relatively simple form, it depends only on the magnitude of momenta and one angle. Though in the present work we stay with our calculations below the breakup threshold, this particular form of the propagator will be the most suited form for considering the solution of Eq. (20) above.

The matrix elements of $\hat{T}$ provide input to the calculation of the matrix elements $\langle \mathbf{q}' \varphi_d | U | \mathbf{q}_0 \varphi_d \rangle$ according to Eq. (16). In this integration we choose the z-axis parallel to $\mathbf{q}'$, so that there is no azimuthal angle between $(\mathbf{q}' + \frac{1}{2}\mathbf{q}'')$ and $\mathbf{q}''$. This specific choice ensures that we only need $\hat{T}$ as function of four variables. For the explicit representation of U the following angle variables are needed, together with the magnitude of $\mathbf{q}'$ and $\mathbf{q}''$

$$
\begin{aligned}
x' &= \hat{\mathbf{q}}' \cdot \hat{\mathbf{q}}_0 = \cos\vartheta', \\
x'' &= \hat{\mathbf{q}}' \cdot \hat{\mathbf{q}}'' = \cos\vartheta'',
\end{aligned}
\tag{21}
$$

and the momenta

$$
\begin{aligned}
|\tfrac{1}{2}\mathbf{q}' + \mathbf{q}_0| &= \sqrt{\tfrac{1}{4} q'^2 + q' q_0 x' + q_0^2} = q_0 \sqrt{\tfrac{5}{4} + x'}, \\
|\mathbf{q}' + \tfrac{1}{2}\mathbf{q}_0| &= \sqrt{q'^2 + q' q_0 x' + \tfrac{1}{4} q_0^2} = q_0 \sqrt{\tfrac{5}{4} + x'}, \\
|\tfrac{1}{2}\mathbf{q}' + \mathbf{q}''| &= \sqrt{\tfrac{1}{4} q'^2 + q' q'' x'' + q''^2}, \\
|\mathbf{q}' + \tfrac{1}{2}\mathbf{q}''| &= \sqrt{q'^2 + q' q'' x'' + \tfrac{1}{4} q''^2}.
\end{aligned}
\tag{22}
$$

The explicit expressions for the remaining angles are calculated in Appendix B. The final expression for the elastic scattering amplitude is then given by

$$\begin{aligned}
&\langle \mathbf{q}'\varphi_d|U|\mathbf{q}_0\varphi_d\rangle \\
&\quad = \langle q_0 x'\varphi_d|U|\mathbf{q}_0\varphi_d\rangle \\
&\quad = 2\varphi_d^2\left(q_0\sqrt{\tfrac{5}{4}+x'}\right)\left(E-\frac{q_0^2}{m}(2+x')\right) \\
&\qquad + 2\int_0^\infty dq'' q''^2 \frac{1}{E-\frac{3}{4m}q''^2 - E_d + i\varepsilon} \\
&\qquad \times \int_{-1}^{1} dx'' \int_0^{2\pi} d\varphi'' \varphi_d\left(\sqrt{\tfrac{1}{4}q_0^2 + q_0 q'' x'' + q''^2}\right) \\
&\qquad \times \left\langle \sqrt{q_0^2 + q_0 q'' x'' + \tfrac{1}{4}q''^2}, \frac{q_0 x' + \frac{1}{2}q'' y}{\sqrt{q_0^2 + q_0 q'' x'' + \frac{1}{4}q''^2}}, 1, q'', y|\hat{T}|\mathbf{q}_0\varphi_d\right\rangle. \quad (23)
\end{aligned}$$

From $\langle q_0 x'\varphi_d|U|\mathbf{q}_0\varphi_d\rangle$ we obtain the differential cross section according to Eq. (4), and the total cross section via Eqs. (5) and (6).

3 Calculation of Scattering Observables

For our model calculations Yukawa interactions of Malfliet-Tjon-type [10] are used,

$$V(\mathbf{p}', \mathbf{p}) = \frac{1}{2\pi^2}\left(\frac{V_R}{(\mathbf{p}'-\mathbf{p})^2 + \mu_R^2} - \frac{V_A}{(\mathbf{p}'-\mathbf{p})^2 + \mu_A^2}\right). \quad (24)$$

We study two different types of pairwise forces, a purely attractive Yukawa interaction and a superposition of a short-ranged repulsive and a long-ranged attractive Yukawa interaction. It should be pointed out that we calculate the potentials as functions of vector momenta and thus define the interaction as a truly local force acting in all partial waves. The parameters are given in Table 1, which also lists the corresponding deuteron binding energies. The parameters are chosen such that the deuteron binding energy is close to the experimental one. With these interactions we first solve the Lippmann-Schwinger equation for the fully-off-shell two-nucleon t-matrix directly as function of the vector variables as described in detail in ref. [6]. The resulting t-matrix is then symmetrized to get $t_s(p', p, x; E - (3/4m)q^2)$. We would like to point out that after having solved the

Table 1. Parameters and deuteron binding energy for the Malfliet-Tjon-type potentials. As conversion factor we use units such that $\hbar c = 197.3286$ MeV fm $= 1$. We also use $\hbar^2/m = 41.47$ MeV fm^2

	V_A [MeV fm]	μ_A [fm^{-1}]	V_R [MeV fm]	μ_R [fm^{-1}]	E_d [MeV]
MT-IIIa	−626.8932	1.550	1438.7228	3.11	−2.231
MT-IVa	−65.1776	0.633	–	–	−2.209

Lippmann-Schwinger equation on Gaussian grids for p, p', and x, we solve the integral equation again to obtain the t-matrix at points $x = \pm 1$. Thus, when solving Eq. (15), we do not have to extrapolate numerically to angle points x of $t_s(p', p, x; E - (3/4m)q^2)$, which can very well be located outside the upper or lower boundary of the Gaussian angle grid of the t-matrix.

The fully off-shell t-matrix, $t(p', p, x, E)$, is obtained for each fixed energy on a symmetric momentum grid, which is divided as $(0, p_1) \cup (p_1, p_{\max})$. The intervals contain NP1 and NP2 Gauss points, with typical values of NP1 = 40 and NP2 = 16 points. Typical values for the interval boundaries are $p_1 = 20$ fm^{-1} and $p_{\max} = 60$ fm^{-1}. For the angular integration x 32 Gauss points are sufficient. Since the momentum region which contributes to a solution of the two-body t-matrix is quite different from the region of importance in a three-body calculation, we map our solution for t_s onto a momentum grid relevant for the three-body transition amplitude. This is done by applying the Lippmann-Schwinger equation repeatedly. The t-matrix $t_s(p', p, x, \varepsilon)$ is obtained at energies $\varepsilon = E - (3/4m)q^2$, exactly at the q values needed in the three-body transition amplitude of Eq. (20). For extracting the residue of the two-body t-matrix, Eq. (14), we represent t_s as

$$(E - E_d)t_s \xrightarrow[E \to E_d]{} V|\varphi_d\rangle\langle\varphi_d|V. \tag{25}$$

The Malfliet-Tjon-type potentials support only an s-wave bound state, and thus Eq. (25) reads explicitly

$$(E - E_d)t_s(\mathbf{p}, \mathbf{p}') \xrightarrow[E \to E_d]{} \frac{1}{4\pi} \left\{ \int_0^\infty dp'' p''^2 V_0(p, p'') \varphi_d(p'') \right\} \times \left\{ \int_0^\infty dp'' p''^2 V_0(p', p'') \varphi_d(p'') \right\}, \tag{26}$$

where V_0 is the $l = 0$ component of the potential.

In order to solve Eq. (20) we follow the iterative procedure outlined in ref. [11]. The method consists of first generating the Neumann series of Eq. (20) and then summing up the series using the Padé method [12–14]. We typically need to sum 15–18 terms to obtain a converged result. This is not surprising, since due to the presence of the three-body bound state the Neumann series itself diverges.

The q'-integration in Eq. (20) is cut off at a value of $q_{\max} = 20\,\text{fm}^{-1}$. The integration interval is divided into two parts, $(0, q_1) \cup (q_1, q_{\max})$, in which we use Gaussian quadrature with NQ1 and NQ2 points, respectively. The value for q_1 is chosen to be 5 fm^{-1}. Typical values for NQ1 and NQ2 are 24 and 16. For the distribution of quadrature points we use the maps given in ref. [15]. The x'' integration requires typically at least 18 integration points, while for the φ'' integration 16 points are already sufficient. The p variable is also defined in an interval $(0, p_1) \cup (p_1, p_{\max})$, where p_1 is chosen to be 7 fm^{-1} and $p_{\max} = 30\,\text{fm}^{-1}$. The two intervals contain NP1 and NP2 points, and we usually choose NP1 = NQ1 and NP2 = NQ2, respectively.

When solving Eq. (20) we have to carry out two-dimensional and three-dimensional interpolations on $\hat{t}_s$ and $\hat{T}$. We use the cubic Hermitean splines of ref. [16]. The functional form of those splines is described in detail in Appendix B of this reference and shall not be repeated here. We find these splines very accurate in

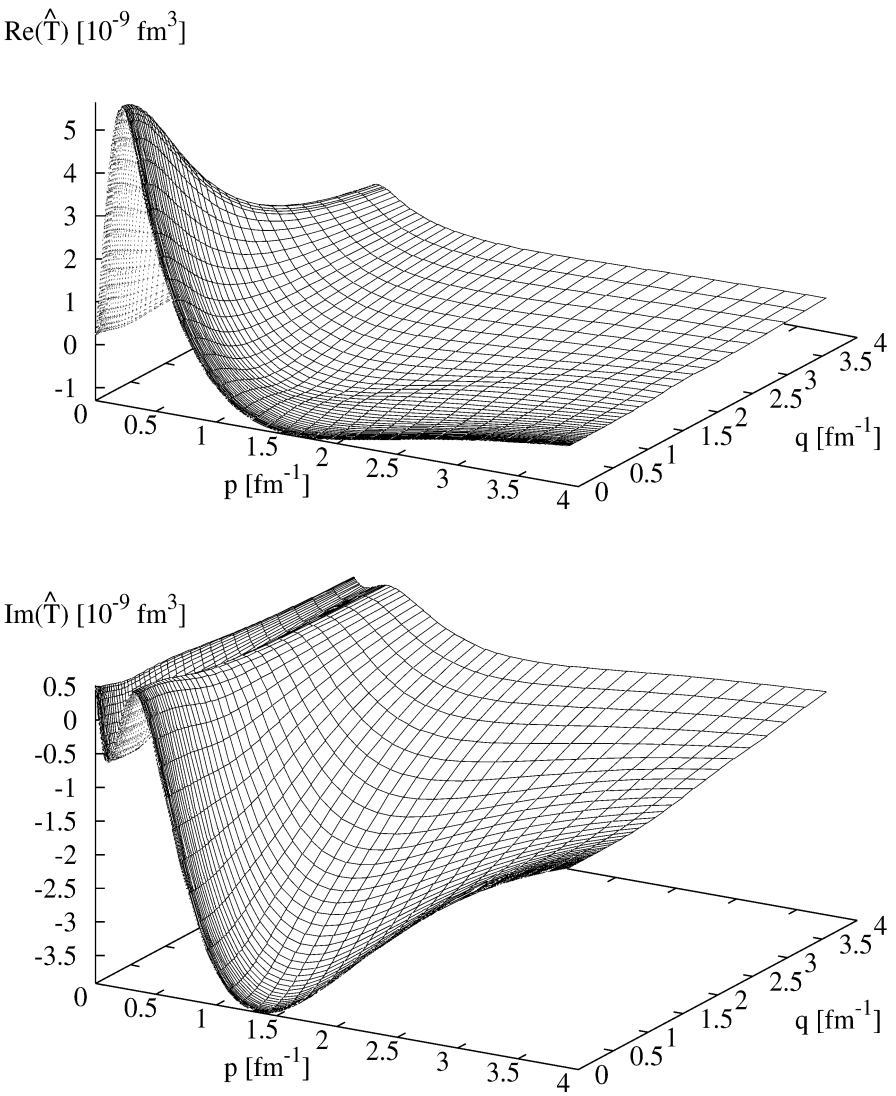

Fig. 1. Real and imaginary part of $\hat{T}(p, x_p = 1, \cos\varphi_{pq} = 1, q, x_q = 1, q_0)$ at 3 MeV projectile energy as obtained from the MT-IVa potential

capturing the peak structure of the two-body t-matrix, which occurs for off-shell momenta $p \simeq p'$. An additional advantage of the cubic Hermitean splines is their computational speed, which is an important factor, since the integral in Eq. (20) requires a very large number of interpolations.

In Fig. 1 the real and the imaginary parts of the scattering amplitude $\hat{T}(p, x_p = 1, \cos\varphi_{pq} = 1, q, x_q = 1, q_0)$ as obtained from the MT-IVa potential are displayed. The projectile energy is 3 MeV, and the amplitude is taken in forward direction, i.e. the two angles are set to zero. The figures show that most of the structure of the amplitude is concentrated at small momenta p and q. The corresponding amplitudes derived from the MT-IIIa potential are shown in Fig. 2.

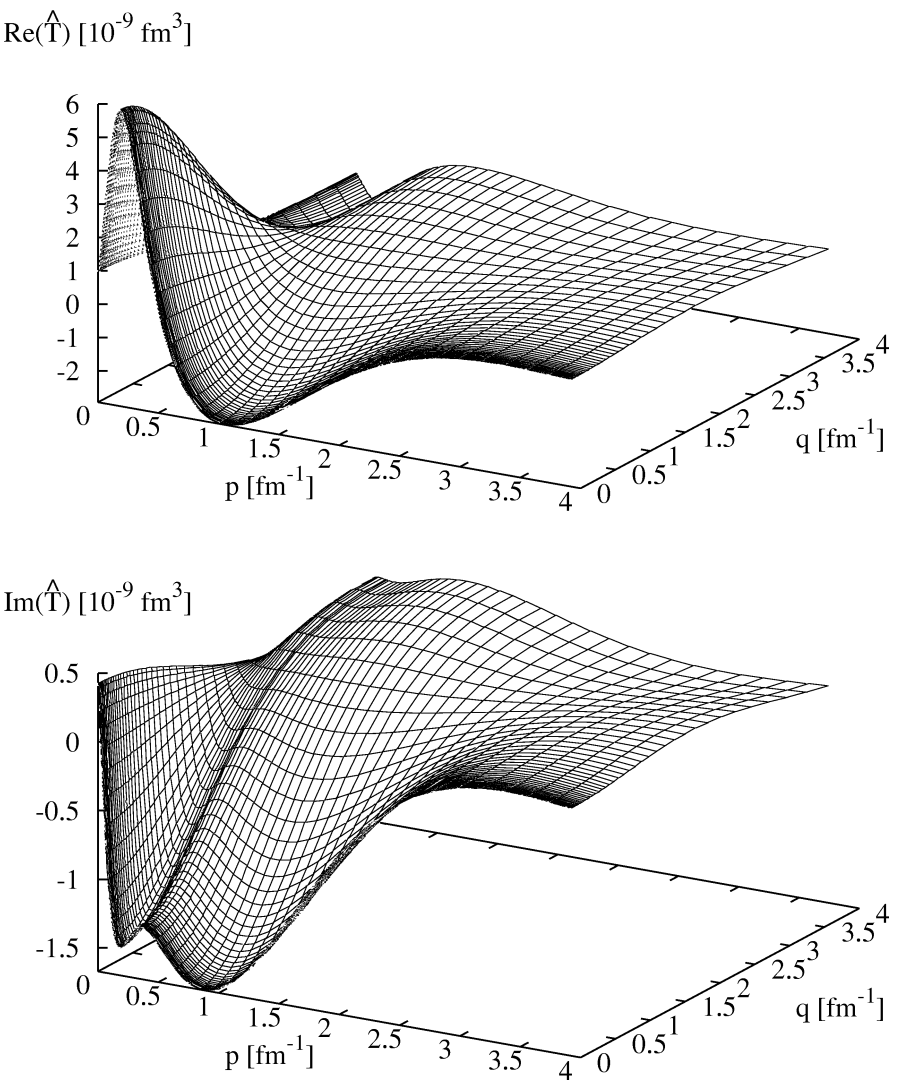

Fig. 2. Same as Fig. 1 but for the MT-IIIa potential

Though the imaginary part has a little more structure for p smaller than 1 fm^{-1}, the function is in general very smooth. The real part of $\hat{T}$ has for both potentials a quite similar structure.

The solution for the transition amplitude serves as basic input to obtain the elastic scattering amplitude according to Eq. (23). In carrying out the integrals we use the same grids as in the integral equation for $\hat{T}$. The differential cross section obtained from the MT-IVa potential is shown in Fig. 3 as function of the projectile laboratory energy E and the scattering angle ϑ for energies from 0.01 MeV to 3.2 MeV. As expected, for very low energies the differential cross section is isotropic, which indicates that in a partial-wave description only s-waves contribute. At about 1 MeV projectile energy the differential cross section starts to develop its more

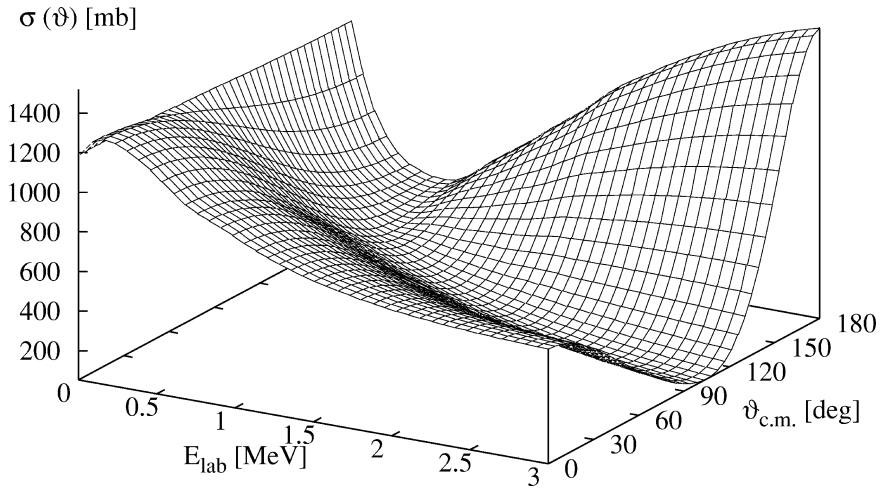

Fig. 3. The differential cross section $\sigma(\vartheta)$ as function of the projectile energy and scattering angle ϑ obtained from the MT-IVa potential

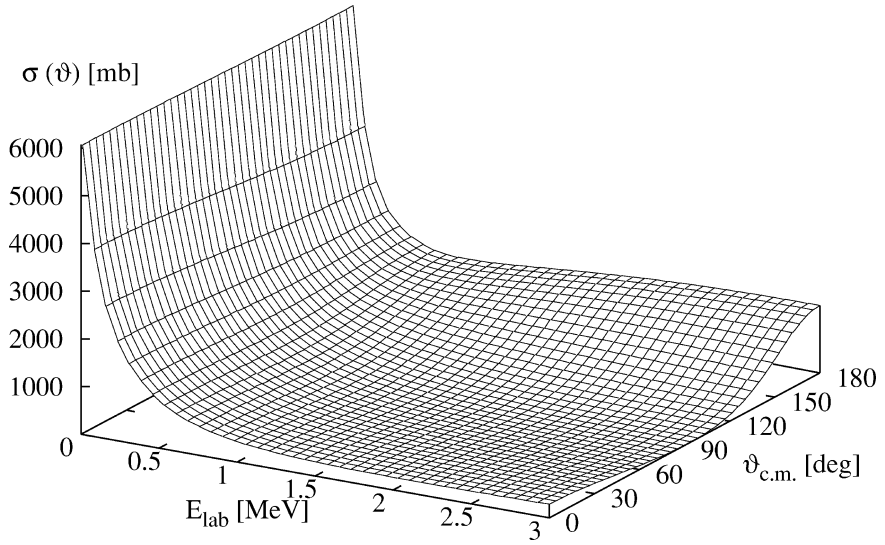

Fig. 4. Same as Fig. 3 but for the MT-IIIa potential

characteristic shape, namely in forward and backward direction and a minimum around $\vartheta = 100°$. In Fig. 4 the differential cross section obtained from the MT-IIIa potential is displayed as function of the projectile energy and the scattering angle. The obvious difference with respect to Fig. 3 is that the magnitude of $\sigma(\vartheta)$ obtained from the MT-IIIa is about 5 times larger than the one obtained from MT-IVa at small energies. The difference is related to the different values of the three-

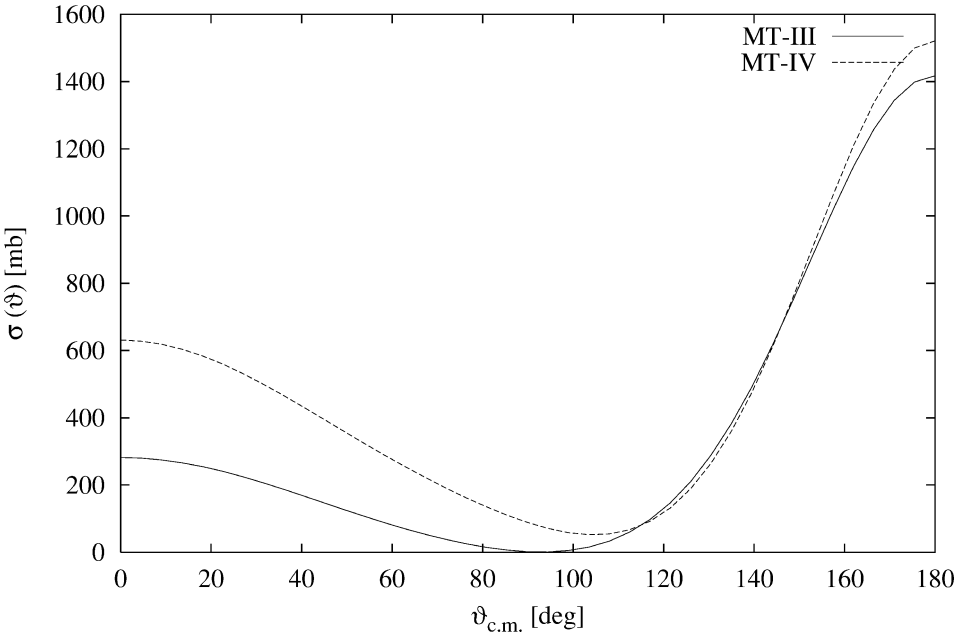

Fig. 5. The differential cross section $\sigma(\vartheta)$ at 3 MeV projectile energy obtained from the MT-IIIa potential (solid line) and the MT-IVa potential (dashed line)

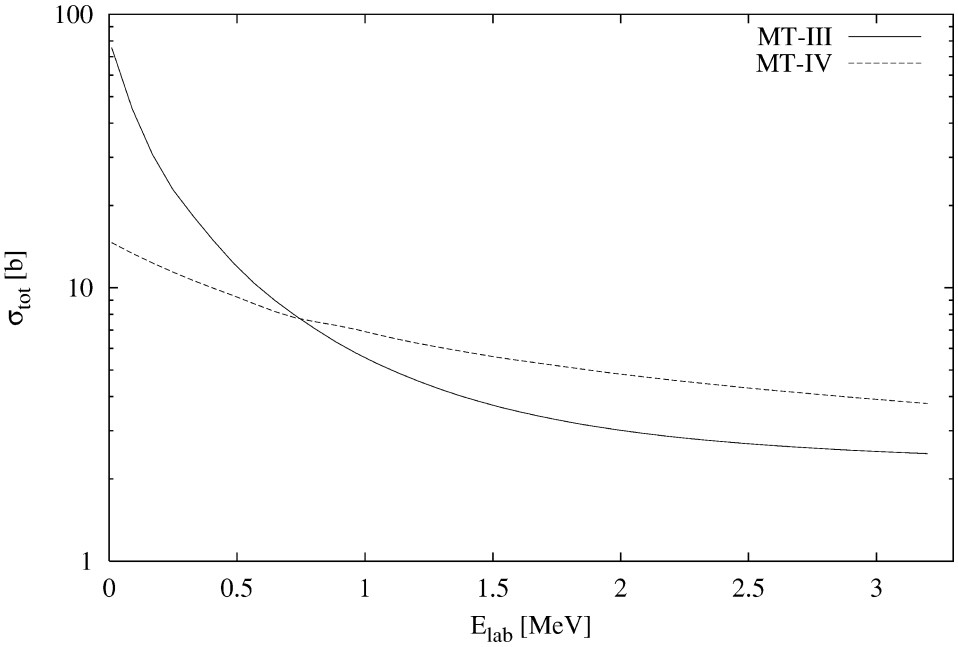

Fig. 6. The total cross sections $\sigma_{\rm tot}$ as function of the projectile energy obtained from the MT-IIIa potential (solid line) and the MT-IVa potential (dashed line)

body scattering length for the different potentials. The one for MT-IIIa turns out to be 2.034 fm and is much larger than the one for MT-IVa, which is 0.887 fm. These numbers are related to the different three-body binding energies, which are

-19.8625 MeV for the MT-IIIa potential and -25.1632 MeV for the MT-IVa potential. According to ref. [17] the scattering length can be calculated via

$$a = \frac{2\pi}{3} m \langle \mathbf{q}_0 \varphi_d | U | \mathbf{q}_0 \varphi_d \rangle \Big|_{q_0=0} . \tag{27}$$

Due to the different scale the onset of a deviation from the isotropic $\sigma(\vartheta)$ is not so easily visible in Fig. 4, but it also occurs at about 1 MeV. In order to better compare the differential cross section obtained from both potentials, this observable is shown in Fig. 5 at 3 MeV for both potentials as function of the scattering angle. Here one can see that $\sigma(\vartheta)$ is larger especially in forward direction for the purely attractive potential MT-IVa. This behavior is even clearer visible in Fig. 6, where the total cross sections $\sigma_{\rm tot}$ obtained from MT-IIIa and MT-IVa are shown as function of energy.

For demonstrating and discussing the numerical stability and accuracy of our algorithm we choose the MT-IVa potential and a fixed energy and discuss the behavior of the observables as function of the grid points. Table 2 contains the total cross section calculated at 3 MeV using Eq. (5) and also via the optical theorem,

Table 2. The total cross section for the MT-IVa potential at 3.0 MeV. The numbers of grid points for $\hat{T}$ are NQ = NQ1 + NQ2, NP = NP1 + NP2, NXP, and NXQ as explained in the text. The grid points for the integration are NX″ and Nφ″. The grids for the t-matrix are denoted with NP$_t$ and NX$_t$

NQ	NP	NXP	NXQ	NX″	Nφ″	NP$_t$	NX$_t$	$\sigma_{\rm tot}^{\rm int.}$	$\sigma_{\rm tot}^{\rm opt.}$
30	30	18	14	18	10	40	40	3903.18	3906.53
30	30	18	14	18	16	40	40	3909.12	3913.19
30	30	18	14	18	20	40	40	3909.22	3913.95
30	30	18	18	18	20	40	40	3909.93	3914.09
30	30	18	22	18	20	40	40	3910.06	3914.09
30	30	22	22	18	20	40	40	3909.73	3914.00
30	38	22	22	18	20	40	40	3909.66	3914.30
30	42	22	22	18	20	40	40	3909.11	3913.45
38	42	22	22	18	20	40	40	3916.66	3921.11
42	42	22	22	18	20	40	40	3913.17	3917.47
46	42	22	22	18	20	48	40	3911.16	3915.16
46	42	22	22	18	20	56	40	3911.13	3915.02
46	42	22	22	18	20	64	40	3911.11	3914.96
50	42	22	22	18	20	64	40	3911.15	3915.06
50	42	22	22	24	20	64	40	3910.88	3915.04
50	50	22	22	24	20	64	40	3910.78	3914.93
50	50	22	22	24	22	72	40	3910.79	3914.88
50	50	22	22	24	22	80	40	3910.71	3914.72
50	50	22	22	24	22	80	40	3910.71	3914.69
58	58	22	22	24	22	80	40	3913.31	3917.22
58	58	26	26	24	26	80	40	3913.95	3917.44
58	58	30	30	24	26	80	40	3913.85	3917.44
58	58	34	34	24	26	80	40	3913.85	3917.46
58	58	38	38	24	26	80	40	3913.86	3917.61

Eq. (6). The first calculations listed in the table are performed with a moderate amount of grid points in all variables. We then successively increase the points of one variable at a time and see that the variation in the total cross section stays about 0.3%. From this we conclude that our algorithm is very stable, and the numerical error, which necessarily has to occur due to the large number of interpolations, is certainly not higher than 1%.

We choose to consider the total cross section for this stability study, since state-of-the-art measurements of the total cross section have an accuracy of about 0.5% [18]. We also see the different ways of calculating $\sigma_{\rm tot}$ differ consistently by about 0.2%, almost independent of the number of grid points used. From this we can conclude that the general error of our calculation is 0.5% or lower, which is for all practical purposes sufficiently accurate. A further test of the accuracy and convergence of our numerical calculation is in the insertion of our converged solution for the transition amplitude $\hat{T}$ a further time into Eq. (20) and then recalculate the observables with this new solution for $\hat{T}$. The comparison is carried out for the differential cross section at 3 MeV and listed in Table 3. Here we used the results of the calculation with the highest number of points from Table 2, but results for the other calculations are similar. As can be seen the agreement of the two calculations is excellent, and we conclude that our calculations are properly converged.

Table 3. The differential cross section for the MT-IVa potential at 3.0 MeV. The second column contains the cross section obtained from the Padé sum and the third column the cross section obtained by reinserting the solution. The corresponding total cross sections are 3913.86 mb and 3913.93 mb, respectively

ϑ [deg]	$\sigma(\vartheta)$ [mb]	$\sigma(\vartheta)$ [mb]
0.000	634.458	634.483
8.215	624.423	624.446
17.548	590.018	590.040
26.893	535.377	535.396
36.240	467.039	467.056
45.589	392.139	392.153
54.938	316.841	316.853
64.288	245.326	245.336
73.638	180.241	180.249
82.988	123.550	123.557
92.337	78.909	78.917
101.687	53.890	53.899
111.037	61.678	61.690
120.387	120.744	120.760
129.736	250.915	250.937
139.085	464.483	464.511
148.434	752.825	752.860
157.780	1074.342	1074.383
167.122	1354.729	1354.775
176.421	1508.989	1509.036
180.000	1522.727	1522.774

4 A Second Choice of Variables for the Scattering Equations

In Sect. 2 we described our choice of the coordinate system used to solve the integral equation, Eq. (13), for the transition amplitude T. There we choose the z-axis for the integration parallel to $\mathbf{q}$, which has the advantage of giving the free propagator in the kernel a relatively simple functional form. It also led to Eq. (20) being a three-dimensional integral equation in 4 variables. Obviously, the above-described choice is not the only one. In order to test our calculations we additionally solve Eq. (13) with a different choice of coordinate systems. For this specific calculation we choose the z-axis for the overall coordinate system to be parallel to $\mathbf{q}_0$ as well as for the integration in Eq. (13). Due to the rotational invariance of the problem we can choose the azimuthal angle between those 2 coordinate systems to be zero. With these assumptions the variables necessary to explicitly express Eq. (20) are

$$\begin{aligned}
p &= |\mathbf{p}|, \\
q &= |\mathbf{q}|, \\
x_p &= \hat{\mathbf{p}} \cdot \hat{\mathbf{q}}_0, \\
x_q &= \hat{\mathbf{q}} \cdot \hat{\mathbf{q}}_0, \\
\cos\varphi_{pq} &= \cos\varphi(\mathbf{p},\mathbf{q}) = \hat{\mathbf{p}}_{xy} \cdot \hat{\mathbf{q}}_{xy}, \\
y_q &= \hat{\mathbf{q}} \cdot \hat{\mathbf{q}}'' = x_q x'' + \sqrt{1-x_q^2}\sqrt{1-x''^2}\cos\varphi'', \\
y_p &= \hat{\mathbf{p}} \cdot \hat{\mathbf{q}}'' = x_p x'' + \sqrt{1-x_p^2}\sqrt{1-x''^2}\cos(\varphi_{pq}-\varphi''), \\
q'' &= |\mathbf{q}''|, \\
x'' &= \hat{\mathbf{q}}'' \cdot \hat{\mathbf{q}}_0, \\
\cos\varphi'' &= \cos\varphi''(\mathbf{q}'',\mathbf{q}).
\end{aligned} \tag{28}$$

The calculation of the remaining angles and momenta is straightforward and similar to the ones given in Sect. 2. Thus they are not given here. Using the above definitions of the variables we finally arrive at the explicit expression for the transition amplitude $\hat{T}$

$$\begin{aligned}
&\langle p, x_p, \cos\varphi_{pq}, q, x_q | \hat{T} | \mathbf{q}_0 \varphi_d \rangle \\
&\quad = \varphi_d\left(\sqrt{q^2 + qq_0x_q + \tfrac{1}{4}q_0^2}\right) \\
&\qquad \times \hat{t}_s\left(p, \sqrt{\tfrac{1}{4}q^2 + qq_0x_q + q_0^2}, \frac{\frac{1}{2}qx_{pq} + q_0x_p}{\sqrt{\frac{1}{4}q^2 + qq_0x_q + q_0^2}}; E - \frac{3}{4m}q^2\right) \\
&\qquad + \int_0^\infty dq''q''^2 \int_{-1}^1 dx'' \int_0^{2\pi} d\varphi'' \, \frac{1}{E - \frac{1}{m}(q^2 + qq''y_q + q''^2)}
\end{aligned}$$

$$\times \hat{t}_s\left(p, \sqrt{\tfrac{1}{4}q^2 + qq''y_q + q''^2}, \frac{\frac{1}{2}qx_{pq} + q''y_p}{\sqrt{\frac{1}{4}q^2 + qq''y_q + q''^2}}; E - \frac{3}{4m}q^2\right)$$
$$\times \frac{\left\langle \sqrt{q^2 + qq''y_q + \frac{1}{4}q''^2}, \frac{qx_q + \frac{1}{2}q''x''}{\sqrt{q^2 + qq''y_q + \frac{1}{4}q''^2}}\cos\tilde{\varphi}, q'', x''|\hat{T}|\mathbf{q}_0\varphi_d\right\rangle}{E - \frac{3}{4m}q''^2 - E_d + i\varepsilon}. \tag{29}$$

As in Eq. (20) we solve for $\hat{T}$, where the residue at the deuteron pole is explicitly taken into account as described in Eq. (14). In the form of Eq. (29) the three-body propagator has an explicit angle dependence. In addition one has a three-dimensional integral depending on five variables. The latter makes the numerical solution an order of magnitude more time-consuming. Thus Eq. (29) is solved on similar grids as Eq. (20), however with fewer grid points.

After solving for $\hat{T}$, we obtain the elastic scattering amplitude by employing Eq. (16). Using the same coordinate system, namely the z-axis being parallel to $\mathbf{q}_0$, the explicit expression for U reads

$$\begin{aligned}
\langle \mathbf{q}'\varphi_d|U|\mathbf{q}_0\varphi_d\rangle &= \langle q_0x'\varphi_d|U|\mathbf{q}_0\varphi_d\rangle \\
&= 2\varphi_d^2\left(q_0\sqrt{\tfrac{5}{4}+x'}\right)\left(E - \frac{q_0^2}{m}(2+x')\right) \\
&\quad + 2\int_0^\infty dq''q''^2\frac{1}{E - \frac{3}{4m}q''^2 - E_d + i\varepsilon} \\
&\quad \times \int_{-1}^{1}dx''\int_0^{2\pi}d\varphi''\varphi_d\left(\sqrt{\tfrac{1}{4}q_0^2 + q_0q''y + q''^2}\right) \\
&\quad \times \left\langle \sqrt{q_0^2 + q_0q''y + \tfrac{1}{4}q''^2}, \frac{q_0x' + \frac{1}{2}q''x''}{\sqrt{q_0^2 + q_0q''y + \frac{1}{4}q''^2}}, \cos\tilde{\varphi}, q'', x''|\hat{T}|\mathbf{q}_0\varphi_d\right\rangle.
\end{aligned} \tag{30}$$

Here $x' = \hat{\mathbf{q}}' \cdot \hat{\mathbf{q}}_0$ and $y = \hat{\mathbf{q}}' \cdot \hat{\mathbf{q}}''$. The calculation of the azimuthal angle $\tilde{\varphi}$ between $(\mathbf{q} + \frac{1}{2}\mathbf{q}'')$ and $\mathbf{q}''$ is more complicated and given in Appendix C.

It should be clear from the beginning that the solution of Eq. (29) is not only much more time-consuming, but will also a priori contain a larger numerical error due to the increased number of interpolations. In addition four-dimensional interpolations are required, whereas for the solution of Eq. (20) the maximum dimension for the interpolation is three. In Fig. 7 we compare the differential cross sections at 3.0 MeV obtained from both algorithms using a medium number of grid points only. As an aside, solving Eq. (29) with the same high number of grid points as in Eq. (20) is too expensive, especially since we only had in mind to perform a rough comparison of the two schemes. Thus, we also did not perform the same amount of accuracy tasks as described in Sect. 3 for the solution of Eq. (20). As seen in Fig. 7, both solutions are reasonably close, and the accuracy is good enough to establish that in general both methods give similar results. However, for practical calculations, the procedure described in this section should not be recommended.

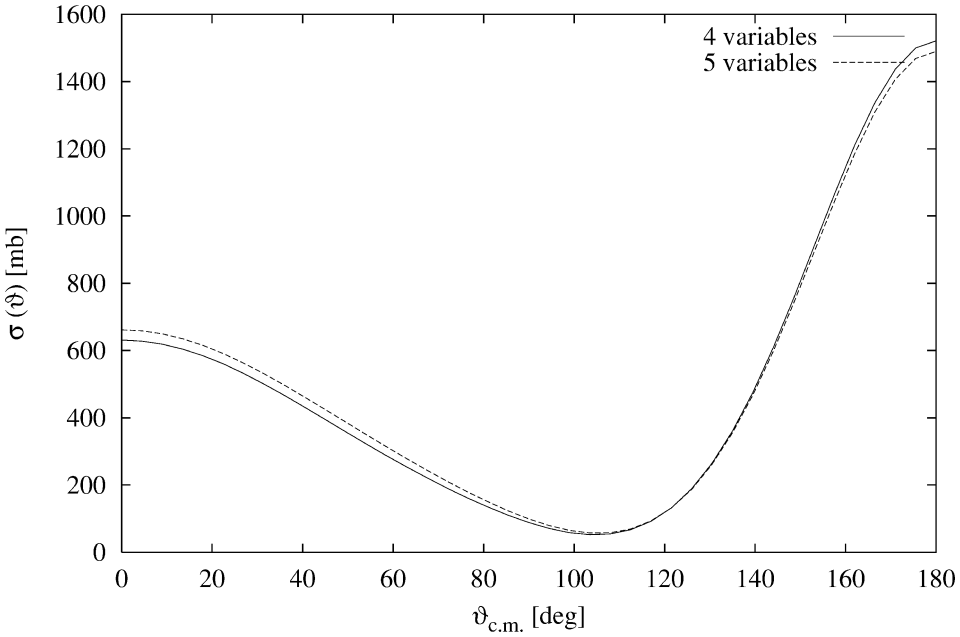

Fig. 7. The differential cross section obtained from the MT-IVa potential at 3.0 MeV based on the solution of $\hat{T}$ using four variables (solid line) and using five variables (dashed line). The explanation of the calculations is given in the text

5 Summary

An alternative approach to the state-of-the-art three-nucleon scattering calculations, which are based on solving the Faddeev equations in a partial wave basis, is to work directly with momentum vector variables. We formulate the three-body scattering equations below the three-body breakup threshold for identical particles as function of vector Jacobi momenta and the projectile momentum, specifically the magnitudes of the momenta and the angles between them. We would like to point out that our specific formulation and the choices of coordinate systems are also applicable above the breakup threshold. However, here the logarithmic singularities, inherent to the breakup, have to be treated explicitly.

As two-body force we concentrate on a superposition of an attractive and a repulsive Yukawa interaction, which is typical for nuclear physics, as well as on an attractive Yukawa interaction. The corresponding two-body t-matrices, which enter the Faddeev equations, were also calculated as function of vector momenta. We neglected spin degrees of freedom in all our calculations.

In order to obtain scattering observables, which are in our case the differential and the total cross section, one solves first an integral equation for the transition amplitude $\hat{T}$. The scattering amplitude is then obtained by an additional integration over the half-shell amplitude T. This set of equations contains in essence four vector momenta, the projectile momentum, the Jacobi momenta, and a momentum vector as integration variable in the kernel. In principle, one has different choices of the coordinate system, in which the calculations are carried out. We present different choices, one leading to a three-dimensional integral equation in four

variables for the transition amplitude $\hat{T}$ and one leading to a three-dimensional integral equation in five variables for $\hat{T}$. Obviously, the first choice is the preferred one. It has the additional advantage that the free three-body propagator acquires a relatively simple form, which will become relevant considering scattering above the breakup threshold.

Using the transition amplitude given as function of four variables we calculate the observables for different projectile energies and test the accuracy and stability of our algorithms. We establish that our calculations have an overall accuracy of less than 0.5%, which is sufficient for all practical purposes, i.e. comparison with experimental measurements. We also calculate the scattering observables at one energy using the transition amplitude given as function of five variables. The two different algorithms are in qualitative agreement, which gives us confidence that our calculation is correct.

Summarizing we can state that the Faddeev equations for scattering below the breakup threshold can be handled in a straightforward and numerically reliable fashion when using vector momenta as variables. Our formulation allows to treat the logarithmic singularities above the breakup threshold in a straightforward fashion, and work along this line is in progress.

Acknowledgement. This work was performed in part under the auspices of the U.S. Department of Energy under contract no. DE-FG02-93ER40756 with Ohio University, the NATO Collaborative Research Grant 960892, and the National Science Foundation under Grant No. INT-9726624. We thank the Ohio Supercomputer Center (OSC) for the use of their facilities under Grant No. PHS206, the National Energy Research Supercomputer Center (NERSC) for the use of their facilities under the FY1998 Massively Parallel Processing Access Program.

Appendix A. Variables for the Transition Amplitude T

In this case we need to rotate around the $y = y''$ axis by the angle ϑ_q. The vectors needed in the new coordinate system are

$$\mathbf{Q}_0 = R(\vartheta_q)\mathbf{q}_0 = \begin{pmatrix} \cos\vartheta_q & 0 & -\sin\vartheta_q \\ 0 & 1 & 0 \\ \sin\vartheta_q & 0 & \cos\vartheta_q \end{pmatrix} \mathbf{q}_0 = q_0 \begin{pmatrix} -\sin\vartheta_q \\ 0 \\ \cos\vartheta_q \end{pmatrix}, \quad \mathbf{Q}'' = q'' \begin{pmatrix} \sin\vartheta''\cos\varphi'' \\ \sin\vartheta''\sin\varphi'' \\ \cos\vartheta'' \end{pmatrix}, \tag{A.1}$$

$$\mathbf{P} = R(\vartheta_q)\mathbf{p} = p \begin{pmatrix} \cos\vartheta_q \sin\vartheta_p - \sin\vartheta_q \cos\vartheta_p \\ 0 \\ \sin\vartheta_q \sin\vartheta_p + \cos\vartheta_q \cos\vartheta_p \end{pmatrix}. \tag{A.2}$$

It is then straightforward to obtain the following angles:

$$\begin{aligned} y_p &= \hat{\mathbf{P}} \cdot \hat{\mathbf{Q}}'' = x'' x_{pq} + \sqrt{1-x''^2}\left(x_q\sqrt{1-x_p^2} - x_p\sqrt{1-x_q^2}\right)\cos\varphi'', \\ y_{q_0} &= \hat{\mathbf{Q}}'' \cdot \hat{\mathbf{Q}}_0 = x_q x'' - \sqrt{1-x_q^2}\,\sqrt{1-x''^2}\cos\varphi'', \\ \hat{\mathbf{P}} \cdot \left(\tfrac{1}{2}\widehat{\mathbf{Q}+\mathbf{Q}''}\right) &= \frac{\frac{1}{2}qx_{pq} + q''y_p}{\sqrt{\frac{1}{4}q^2 + qq''x'' + q''^2}}, \\ \hat{\mathbf{Q}}_0 \cdot \left(\widehat{\mathbf{Q}+\tfrac{1}{2}\mathbf{Q}''}\right) &= \frac{qx_q + \frac{1}{2}q''y_{q_0}}{\sqrt{q^2 + qq''x'' + \frac{1}{4}q''^2}}. \end{aligned} \tag{A.3}$$

Appendix B. Angles for the Scattering Amplitude U

We need the angle between $\hat{\mathbf{q}}_0$ and $\hat{\mathbf{q}}''$. It can be calculated in terms of the integration variables in the new coordinate system. We have chosen the z-axis for the integration being in the x-z plane of the original coordinate system, and the azimuthal angle between them is zero. To get to the new coordinate system we only need to rotate around the $y = y''$ axis by the angle ϑ' using the rotation matrix

$$R(\vartheta') = \begin{pmatrix} \cos\vartheta' & 0 & -\sin\vartheta' \\ 0 & 1 & 0 \\ \sin\vartheta' & 0 & \cos\vartheta' \end{pmatrix}. \tag{B.1}$$

The two vectors in the new coordinate system are given by

$$\mathbf{Q}_0 = R(\vartheta')\mathbf{q}_0 = q_0 \begin{pmatrix} -\sin\vartheta' \\ 0 \\ \cos\vartheta' \end{pmatrix}, \qquad \mathbf{Q}'' = R(\vartheta_q)q'' = q'' \begin{pmatrix} \sin\vartheta''\cos\varphi'' \\ \sin\vartheta''\sin\varphi'' \\ \cos\vartheta'' \end{pmatrix}. \tag{B.2}$$

The angle between them is

$$\begin{aligned} y = \hat{\mathbf{Q}}'' \cdot \hat{\mathbf{Q}}_0 &= -\sin\vartheta'\sin\vartheta''\cos\varphi'' + \cos\vartheta'\cos\vartheta'' \\ &= x'x'' - \sqrt{1-x'^2}\,\sqrt{1-x''^2}\cos\varphi''. \end{aligned} \tag{B.3}$$

The other angle we are looking for is

$$\hat{\mathbf{Q}}_0 \cdot \left(\widehat{\mathbf{Q}' + \tfrac{1}{2}\mathbf{Q}''}\right) = \frac{q_0 x' + \frac{1}{2}q''y}{\sqrt{q_0^2 + q_0 q'' x'' + \frac{1}{4}q''^2}}. \tag{B.4}$$

Appendix C. Angles in the Five-Dimensional Case

We are looking for the azimuthal angle $\tilde{\varphi}$ between $(\mathbf{q} + \frac{1}{2}\mathbf{q}'')$ and $\mathbf{q}''$. We had chosen $\mathbf{q}$ being in the x-z plane, now one can find the azimuthal angle $\tilde{\varphi}$ by going into the x-y plane and using the cosine theorem

$$|\mathbf{q}_{xy}|^2 = \left|\tfrac{1}{2}\mathbf{q}''_{xy}\right|^2 + \left|\left(\mathbf{q} + \tfrac{1}{2}\mathbf{q}''\right)_{xy}\right|^2 - 2\left|\tfrac{1}{2}\mathbf{q}''_{xy}\right|\left|\left(\mathbf{q} + \tfrac{1}{2}\mathbf{q}''\right)_{xy}\right|\cos\tilde{\varphi}. \tag{C.1}$$

The components of the vectors in the x-y plane are given by

$$\begin{aligned} |\mathbf{q}_{xy}| &= q\sin\vartheta_q = q\sqrt{1-x_q^2}, \\ \left|\tfrac{1}{2}\mathbf{q}''_{xy}\right| &= \tfrac{1}{2}q''\sin\vartheta_{q''} = \tfrac{1}{2}q''\sqrt{1-x''^2}, \\ \left|\left(\mathbf{q} + \tfrac{1}{2}\mathbf{q}''\right)_{xy}\right| &= \left|\mathbf{q} + \tfrac{1}{2}\mathbf{q}''\right|\sin\vartheta_{\mathbf{q}_0,\left(\frac{1}{2}\mathbf{q}''+\mathbf{q}\right)} = \left|\mathbf{q} + \tfrac{1}{2}\mathbf{q}''\right|\sqrt{1-x_1^2} \end{aligned} \tag{C.2}$$

with

$$x_1 = \hat{\mathbf{q}}_0 \cdot \left(\widehat{\mathbf{q} + \tfrac{1}{2}\mathbf{q}''}\right) = \frac{\frac{1}{2}q''x'' + qx_q}{\left|\mathbf{q} + \frac{1}{2}\mathbf{q}''\right|}. \tag{C.3}$$

Inserting these relations in Eq. (C.1) we find

$$\cos\tilde{\varphi} = \frac{\frac{1}{4}q''^2(1-x''^2) + \left|\mathbf{q} + \frac{1}{2}\mathbf{q}''\right|^2(1-x_1^2) - q^2(1-x_q^2)}{q''\sqrt{1-x''^2}\left|\mathbf{q} + \frac{1}{2}\mathbf{q}''\right|\sqrt{1-x_1}}, \tag{C.4}$$

which can be simplified to the final result

$$\cos\tilde{\varphi} = \frac{\frac{1}{2}q''\sqrt{1-x''^2} + q\sqrt{1-x_q^2}\cos\varphi''}{\sqrt{\frac{1}{4}(q''\sqrt{1-x''^2})^2 + (q\sqrt{1-x_q^2})^2 + (q''\sqrt{1-x''^2})(q\sqrt{1-x_q^2})\cos\varphi''}}. \tag{C.5}$$

References

1. Arriaga, A., Pandharipande, V. R., Wiringa, R. B.: Phys. Rev. **C52**, 2362 (1995)
2. Carlson, J.: Phys. Rev. **C36**, 2026 (1987)
3. Carlson, J.: Phys. Rev. **C38**, 1879 (1988)
4. Zabolitzki, J. G., Schmidt, K. E., Kalos, M. H.: Phys. Rev. **C25**, 1111 (1982)
5. Carlson, J., Schiavilla, R.: Rev. Mod. Phys. **70**, 743 (1998)
6. Elster, Ch., Thomas, J. H., Glöckle, W.: Few-Body Systems **24**, 55 (1998)
7. Machleidt, R., Holinde, K., Elster, Ch.: Phys. Rep. **149**, 1 (1987)
8. Elster, Ch., Schadow, W., Nogga, A., Glöckle, W.: Few-Body Systems **27**, 83 (1999)
9. Glöckle, W., Witała, H., Hüber, D., Kamada, H., Golak, J.: Phys. Rep. **274**, 107 (1996)
10. Malfliet, R. A., Tjon, J. A.: Nucl. Phys. **A127**, 161 (1969)
11. Kloet, W. M., Tjon, J. A.: Ann. Phys. (NY) **79**, 407 (1973)
12. Baker, G. A., Gammel, J. L. (eds.): The Padé Approximant in Theoretical Physics. New York: Academic Press 1970
13. Glöckle, W.: The Quantum Mechanical Few-Body Problem. Berlin-Heidelberg-New York: Springer 1983
14. Hüber, D.: Ph.D. Thesis. Bochum: Bochum University 1996
15. Glöckle, W.: Computational Nuclear Physics, I: Nuclear Structure (Langanke, K., Maruhn, J. A., Koonin, S. E., eds.), p. 152. Berlin-Heidelberg-New York: Springer 1991
16. Hüber, D., Witała, H., Nogga, A., Kamada, W. G. H.: Few-Body Systems **22**, 107 (1997)
17. Hüber, D., et al.: Phys. Rev. **C51**, 1100 (1995)
18. Abfalterer, W. P., et al.: Phys. Rev. Lett. **81**, 57 (1998)

Received March 9, 1999; revised July 29, 1999; accepted for publication September 6, 1999